Earth and Planetary Science Letters 331–332 (2012) 269–280

Contents lists available at SciVerse ScienceDirect

Earth and Planetary Science Letters

journal homepage: www.elsevier.com/locate/epsl

Tracking slabs beneath northwestern Pacific subduction zones

Yu Jeffrey Gu *, Ahmet Okeler [1], Ryan Schultz [1]

Department of Physics, University of Alberta, Edmonton, AB, Canada, T6G2E1

ARTICLE INFO

Article history:
Received 11 January 2011
Received in revised form 12 March 2012
Accepted 14 March 2012
Available online xxxx

Editor: P. Shearer

Keywords:
Highly reflective zone
SS precursor
Northwestern Pacific
Stagnant slab
Mantle transition zone
Slab penetration

ABSTRACT

This study uses the amplitudes of bottom-side reflected shear waves to constrain the morphology and dynamics of subducted oceanic lithosphere beneath northwestern Pacific subduction zones. Across Honshu arc, the 410- and 660-km seismic discontinuities are detected at the respective depths of 395 ± 5 and 685 ± 5 km within the Wadati–Benioff zone. Their topographies are negatively correlated along slab dip, showing the dominant effect of temperature on the olivine phase changes within the upper mantle transition zone. The base of the upper mantle shows broad depressions as well as localized zones of shallow/average depths beneath Korea and northeast China. The 15 + km peak-to-peak topography west of the Wadati–Benioff zones suggests that the stagnant part of the subducted Pacific plate is not as flat as previously suggested. Eastward slab 'pile-up' is also possible at the base of the upper mantle. Across southern Kuril arc, the shear wave reflection coefficients of major olivine phase boundaries fall below 5% within the Wadati–Benioff zone. The apparent reflection gaps and the spatial connection between a strong reflector at ~900 km depth may imply 1) possible compositional variations at the top and bottom of the transition zone and 2) substantial mass/heat flux across the 660-km seismic discontinuity. We also identify strong reflectors within the subducted oceanic lithosphere at mid transition zone depths. The depths and strengths of these reflectors are highly variable between Honshu and southern Kuril islands.

1. Introduction

The convergent boundaries between the Pacific, Amurian, and North American plates are among the fastest destruction zones of old oceanic domains. The subduction process in this region initiated prior to the Eocene epoch (>55 Ma) (Fukao et al., 2001; Northrup et al., 1995) and continues to accommodate regional differential plate motions at the present-day rates of 8–9.5 cm/yr (Bird, 2003; DeMets et al., 1990; Seno et al., 1996). The subducted old oceanic lithospheres are colder than the surrounding mantle, hence are manifested in high velocity anomalies in seismic tomographic images (e.g., Fukao et al., 1992, 2001; Gorbatov and Kennett, 2002; Gorbatov et al., 2000; Grand, 2002; Kárason and van der Hilst, 2000; Lebedev and Nolet, 2003; Li and van der Hilst, 2010; Obayashi et al., 2006; Romanowicz, 2003; van der Hilst et al., 1991, 1997; Widiyantoro et al., 1999; Zhao, 2004; Zhao and Ohtani, 2009). The inferred morphologies and depths of subducted oceanic lithospheres (from here on, 'slabs') vary significantly among the various northwestern segments of the Pacific plate boundary. Parts of the Pacific slab exhibit strong deformations near the base of the upper mantle, e.g., 'pile-up' or stagnation (Fukao et al., 1992, 2001) by as much as 800–1000 km (Huang and Zhao, 2006; Obayashi et al., 2006), while others favor continued descent into the lower mantle (e.g., Fukao et al., 2001, 2009; Gorbatov and Kennett, 2002; Obayashi et al., 2006). Both modes of slab deformation have been corroborated by recent geodynamical calculations that incorporated trench migration and rollback history (Billen, 2010; Nakakuki et al., 2010; Tagawa et al., 2007; Zhu et al., 2010). The interplay between high and low velocities in connection with descending slabs, multi-scale advection (Korenaga and Jordan, 2004; Obayashi et al., 2006) and transition zone slab dehydration (An et al., 2009; Duan et al., 2009; Feng and An, 2010; Lebedev and Nolet, 2003; Li and van der Hilst, 2010; Obayashi et al., 2006; Priesley et al., 2006; Zhao, 2004; Zhao et al., 2007; Zhao and Ohtani, 2009) is inductive to strong gradients in temperature and composition at depths below 250 km.

In addition to seismic tomography, amplitudes and arrival-times of reflected/converted seismic waves from mantle interfaces are effective measures of changes in rock elastic properties. Slab geometry and transition zone thickness are strongly influenced by mineralogical phase transformations of olivine to wadsleyite near 400 km, wadsleyite to ringwoodite near 520 km, and ringwoodite to perovskite + magnesiowustite near 660 km (Akaogi et al., 2007; Bina, 2003 and references therein; Helffrich, 2000; Ita and Stixrude, 1992; Katsura and Ito, 1989). The endothermic phase change at the base of the upper mantle increases local buoyancy forces, which can deflect subducting slabs and cause stagnation (Billen, 2008, 2010; Christensen, 1995; Fukao et al., 2009). Assuming an olivine-rich mantle composition and thermodynamic equilibrium, low temperatures

* Corresponding author. Tel.: +1 780 492 2292; fax: 1 780 492 0714.
E-mail addresses: ygu@ualberta.ca (Y.J. Gu), aokeler@ualberta.ca (A. Okeler), rjs10@ualberta.ca (R. Schultz).
[1] Fax: +1 780 492 0714.

0012-821X/$ – see front matter © 2012 Elsevier B.V. All rights reserved.
doi:10.1016/j.epsl.2012.03.023

from a descending slab are expected to increase the thickness of the transition zone. In fact, broad depressions of the 660-km discontinuity beneath the northwestern Pacific region (e.g., Revenaugh and Jordan, 1991; Shearer and Masters, 1992; Vidale and Benz, 1992) have been widely regarded as crucial observational support for the laboratory experiments.

Among the various observations, bottom-side SH reflections from mantle interfaces known as *SS* precursors (Shearer, 1991; Shearer and Masters, 1992) played a key role in the determination of mantle discontinuity depths. Due to path similarities, the relative times and amplitudes of *SS* and its precursors are sensitive to reflection characteristics beneath the midpoint of the ray path (Fig. 1A). In comparison with converted waves (e.g., Lawrence and Shearer, 2006, 2008; Tauzin et al., 2008; Rondenay, 2009), seismic imaging based on *SS* precursors offers more complete global data coverage (Deuss and Woodhouse, 2002; Flanagan and Shearer, 1998; Gossler and Kind, 1996; Gu and Dziewonski, 2002; Gu et al., 1998; Shearer, 1990, 1991, 1993; Shearer and Masters, 1992; see Deuss, 2009 for review), but their resolving powers at length scales appropriate for slabs have been questioned (Chaljub and Tarantola, 1997; Neele et al., 1997; Shearer et al., 1999). With few exceptions (e.g., Heit et al., 2010; Schmerr and Garnero, 2007), comparisons between shear wave reflectivity and velocity near subduction zones generally emphasized low-degree spherical harmonics (e.g., Gu et al., 2003; Houser and Williams, 2010; Houser et al., 2008; Lawrence and Shearer, 2006; Romanowicz, 2003) and remained qualitative at local length scales.

This study presents new evidence of stagnating and lower-mantle penetrating slabs based on a dense regional dataset of *SS* precursors and effective imaging techniques. Through detailed comparisons of reflection amplitude and high-resolution seismic velocity, we aim to provide a self-consistent, three-dimensional (3D) snapshot of the mantle beneath the northwestern Pacific region. For brevity the following sections will refer to the upper mantle transition zone as MTZ and the associated seismic discontinuities as the 410, 520 and 660.

2. Data and method

In this study we utilize all available broadband, high-gain recordings of earthquakes prior to 2008, a dataset currently managed by the IRIS Data Management Center and contributed by GDSN, IRIS, GEOSCOPE and many other temporary deployments. We only retain shallow (depth<75 km) events to minimize the effect of depth phases, and adopt a magnitude cutoff of Mw>5 to ensure the availability of source mechanisms from GCMT (Dziewonski et al., 1981) for synthetic seismogram computations. We restrict the epicentral distance range to 100°–160° to minimize known waveform interferences from topside reflection and *ScS* precursors (An et al., 2007; Schmerr and Garnero, 2007), and apply a Butterworth band-pass filter with corner periods at 12 s and 75 s. We further eliminate traces with signal-to-noise ratio lower than 3.0 (Gu et al., 2003) and align the resulting traces on the first major swing of *SS*. A constant time shift is subsequently added to each trace based on model predicted *SS-S520S* times to account for variations in crust thickness (Bassin et al., 2000) and surface topography (ETOPO5 database) (e.g., Gu et al., 2003). A reference reflection at 520 km offers an effective compromise between reflections at the 410 and 660 despite a potential depth error of 3–5 km for structures 200–400 km away from the MTZ. Finally, each time sample preceding the reference *SS* time is mapped to a crustal/mantle depth (e.g., Gu et al., 2008; Heit et al., 2010; Zheng et al., 2007) according to travel times predicted by

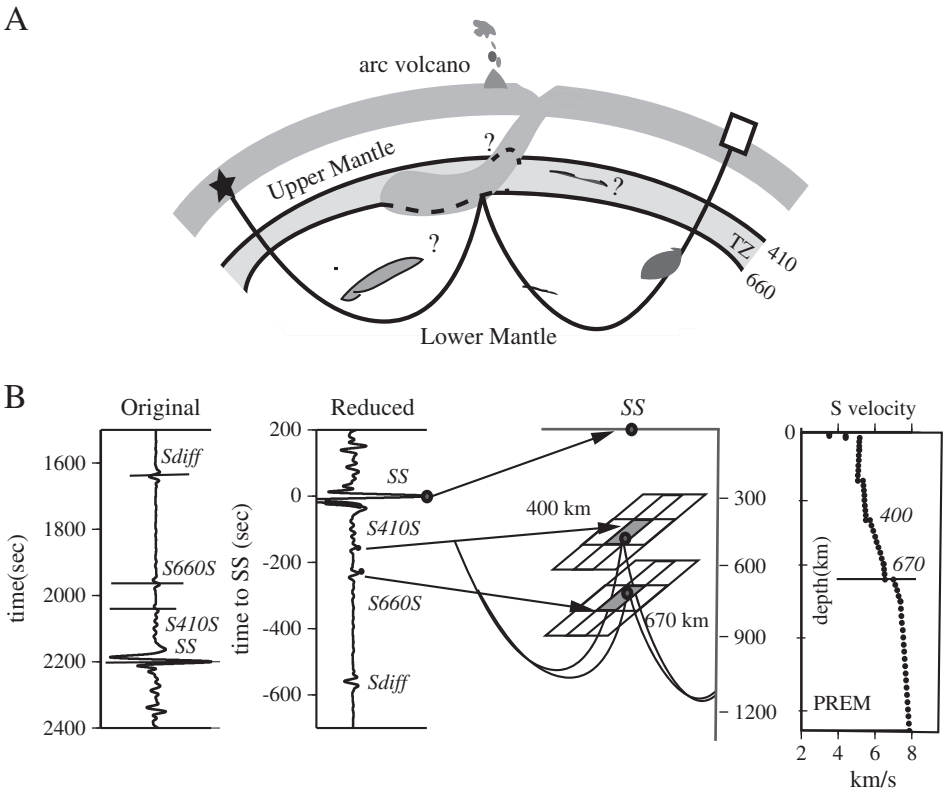

Fig. 1. (A) Schematic drawing of a *SS* precursor reflecting from a subducting oceanic lithosphere at the base of upper mantle. These waves are sensitive to the depths of mantle interfaces and the impedance contrasts across them. (B) Key steps in the time-to-depth conversion of *SS* precursors. By placing the aligned *SS* precursors at the surface (middle), we map a given time sample prior to the arrival of *SS* (left) to the appropriate reflection depth along the predicted differential time curves computed based on PREM (Dziewonski and Anderson, 1981). The right panel shows the isotropic shear velocities of PREM down to 1200-km depth.

PREM (Dziewonski and Anderson, 1981) (Fig. 1B). The sampling rate along the depth axis is 1 km.

Fig. 2 shows the region of interest in this study and 6014 high-quality traces after processing. The ray theoretical reflection points of the precursors are particularly dense in the latitude range of 35°–50°, which enables a direct comparison between southern/central Honshu arc (Profiles A and B) and Kuril trench (Profile C). To obtain a 3D reflectivity image we first partition the study region using a series of equally-spaced, minor-arc cross-sections parallel to Profile A. The perpendicular arc distance between any two cross-sections is 4°, and their end points (hence lengths) vary to reflect the available data coverage. Then, a series of equal-area Common Mid Point (CMP) gathers are populated along each cross-section with section-parallel and section-perpendicular dimensions of 3° and 8°, respectively. These rectangular bins are adopted to maximize the nominal resolutions, especially along the east–west orientation, while ensuring sufficient data in each bin for noise suppression. We subsequently interpolate the resulting migration stacks using a bi-linear method for 3D visualization. Despite linear interpolation used in each spatial direction, bi-linear interpolation is able to construct new data points from a discrete set of original values based on a quadratic function (Press et al., 1992). Finally, Profiles B–D (see Fig. 2) differ from cross-sections used in the 3D construction for a closer examination of the targeted slabs, but the CMP selection strategy and size remain unchanged.

3. Results

3.1. Maps of reflection amplitudes

Stacks of depth-converted *SdS* show large-scale structures in the MTZ and shallow lower mantle. The most prominent structure at the top of the MTZ (Fig. 3A) is an elongated, highly reflective zone (HRZ) that extends from northern Great Khingan Range to Gobi desert in the northwestern corner of the study region. This anomaly reaches a maximum amplitude of 9.5% relative to *SS* (for short, 9.5%) at ~425-km depth (Fig. 3A), approximately 15 km below the global average of the 410 (Gu et al., 2003; Houser et al., 2008), and the limited vertical extent of ~20 km based on 5% reflection amplitude suggests a relative sharp phase transition. A slightly weaker, semi-circular HRZ is further visible in the southwestern corner of the study region, peaking at ~400 km depth and spanning over 1000 km in latitude in northern-central China (see Fig. 3A). The reflection amplitudes of both HRZs are substantially larger than those within the Wadati–Benioff zones (Gudmundsson and Sambridge, 1998) at the respective depths.

The relative reflectivity of Wadati–Benioff zone increases significantly in mid MTZ (Fig. 3B). A wedge-shaped HRZ with 7–8.5% amplitude is observed near the slab corner between Japan and Kuril subduction zones (Gudmundsson and Sambridge, 1998). This is a localized and sharp anomaly, as the reflection amplitude falls below our detection threshold outside the 515–535 km depth range. While sharpness remains consistent, the strengths and lateral dimensions of HRZs are substantially larger at the base of the upper mantle than the depths above (Fig. 3C). At 675 km, major north–south oriented HRZs are present 1) west of the Wadati–Benioff zone, and 2) across eastern Gobi desert (see Fig. 3C). The maximum amplitudes of 9–12% provide strong regional constraints on the nature and depth of major mineralogical phase transition(s). In comparison, HRZs of similar strengths below 850 km (Fig. 3D) require a closer examination. As detailed in the following sections, a dominant north–south oriented HRZ at ~900-km depth along southern Kuril seismogenic zone could have significant implications for the dynamics and mineralogy of the lower mantle.

3.2. Cross-sections of reflectivity and seismic velocity

To explore the relationship between reflection amplitude and seismic velocity, we overlay depth-converted *SS* precursors (Fig. 4) with high-resolution regional *P* velocities (Obayashi et al., 2006). While the use of a regional S velocity would have been ideal, P and S observations are well correlated (Grand, 2002; Romanowicz, 2003) and the

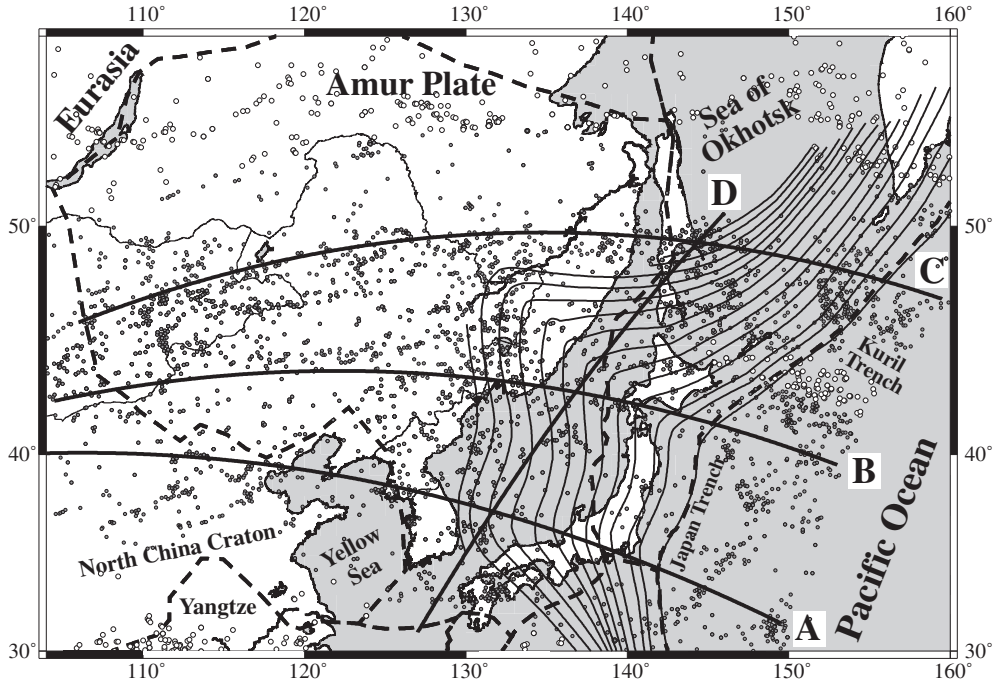

Fig. 2. Ray theoretical surface reflection points of 6014 high-quality *SS* precursors used in this study. The main tectonic elements, plate boundaries (Bird, 2003) and slab contours (Gudmundsson and Sambridge, 1998) are indicated by dashed lines and thin solid lines, respectively; the slab contours are taken at 50 km intervals from the trench. All *SS* bounce points represented by circles contribute to the construction of 3D reflectivity maps (see Fig. 3), while only solid circles are used in the examinations of four vertical Profiles A-D (see Fig. 4).

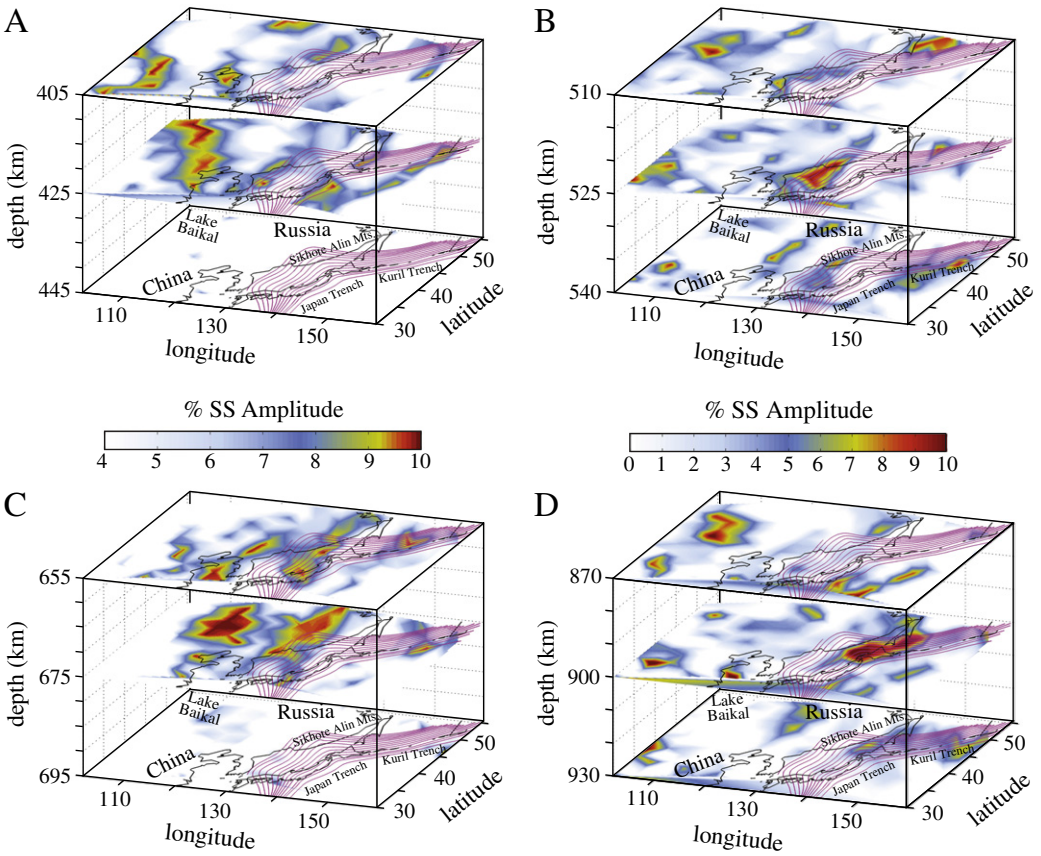

Fig. 3. Interpolated reflectivity maps of *SS* precursor amplitude variations at MTZ (A to C) and shallow lower-mantle (D) depths. The thin magenta lines show the slab contours from Gudmundsson and Sambridge (1998). The viewing angles differ slightly among the four panels. The abbreviation Mt = Mountain. The color bar on the left is used for the reflection maps shown by panels A and C, and the one on the right is used to produce the remaining two panels.

former dataset potentially offers greater spatial resolution in the Pacific Northwest (Fukao et al., 2009). The depth-converted *SS* precursors show clear evidence of sub-horizontal reflectors within depth ranges of 120–180 km, 380–440 km and 630–700 km. The focus of this study is the MTZ and lower mantle where waveform complexities associated with *SS* side-lobes are negligible (e.g., Gu et al., 2003; Shearer, 1993). To ensure the robustness of the key observations, we estimate the uncertainty of the reflectivity profiles based on a bootstrapping resampling algorithm (Efron, 1977) (see Appendix A) and subtract two standard deviations from all data stacks. While this procedure slightly reduces the overall signal strength, reflection amplitudes at the depths with large uncertainties are preferentially suppressed for a more objective assessment.

Profile A (see Fig. 4) shows highly undulating MTZ boundaries between the Pacific Plate and the volcanic arc near central Honshu Island. The 410 east of the Japan trench undergoes 15–20 km local depression relative to the cross-sectional average of 413 ± 5 km. This 500-km wide HRZ reaches the maximum reflection amplitude of ~8% beneath central Honshu arc and overlaps with a *P* wave low-velocity zone between 380 and 400 km depths (Obayashi et al., 2006; see also Bagley et al., 2009; Li and van der Hilst, 2010; Zhao and Ohtani, 2009). The reflection characteristics change sharply towards the Wadati–Benioff zone, where the 410 elevates to ~395 km but loses 3–4% amplitude (see Fig. 4, Profile A). Complex reflective structures are also evident at the base of the MTZ east of Japan trench. The 660 shows 25 + km peak-to-peak topography and the undulations negatively correlate with those of the 410 along trench dip. A deep 660 is observed beneath eastern Sea of Japan (~684 km) and Gulf of Chihli (~675 km), whereas the area in between shows an average or shallow 660 (see Figs. 3C and 4).

The shape of the high-velocity structure becomes quasi-linear near northern Honshu where a significant number of deep-focus earthquakes have been recorded (Fig. 4, Profile B). The 410 remains depressed oceanward from the Wadati–Benioff zone, while a strong HRZ at ~300 km depth approximately marks the top of a *P*-wave low-velocity zone above the MTZ. The reflection characteristics of the 410 in this region are generally consistent with those from central Honshu arc (see Profile A), but the amplitude and depth variations are visibly diminished. A strong 660 is detected at ~645 km depth beneath northern Honshu, which reduces the MTZ width to ~225-km along trench dip (see Fig. 4, Profile B). Further west, the reflectivity profiles shows a broad depression beneath Sea of Japan and Changbai hotspot. This mild depression zone overlaps with high *P* velocities near the base of the MTZ, but appears wider than that expected from 1 + % *P* velocities.

The high-velocity zone beneath Kuril arc (Fig. 4, Profile C) is more complex than those within the two southern profiles. Above-average *P* velocities extend to depths below 750 km along trench dip and across exceptionally weak 410 and 660 (hereafter, 'reflection gap') within the Wadati-Benioff zone. The base of this anomaly, which is interpreted as 0.3–0.5% *P* velocity perturbations, is underlain by an eastward dipping lower-mantle reflector at ~900 km depth (see also Fig. 3D) in the vicinity of the reflection gap. The strength of the 660 gradually increases toward Sikhote-Aline Mountains and effectively outlines the 1 + % *P* velocity zone in the lower half of the MTZ (see Fig. 4, Profile C).

A southwest–northeast transect over the deepest part of the Wadati–Benioff zones (Fig. 4, Profile D) highlights the key reflectivity differences between Japan and Kuril subduction systems. South of Hokkaido corner, large-scale high-velocity structures are mainly

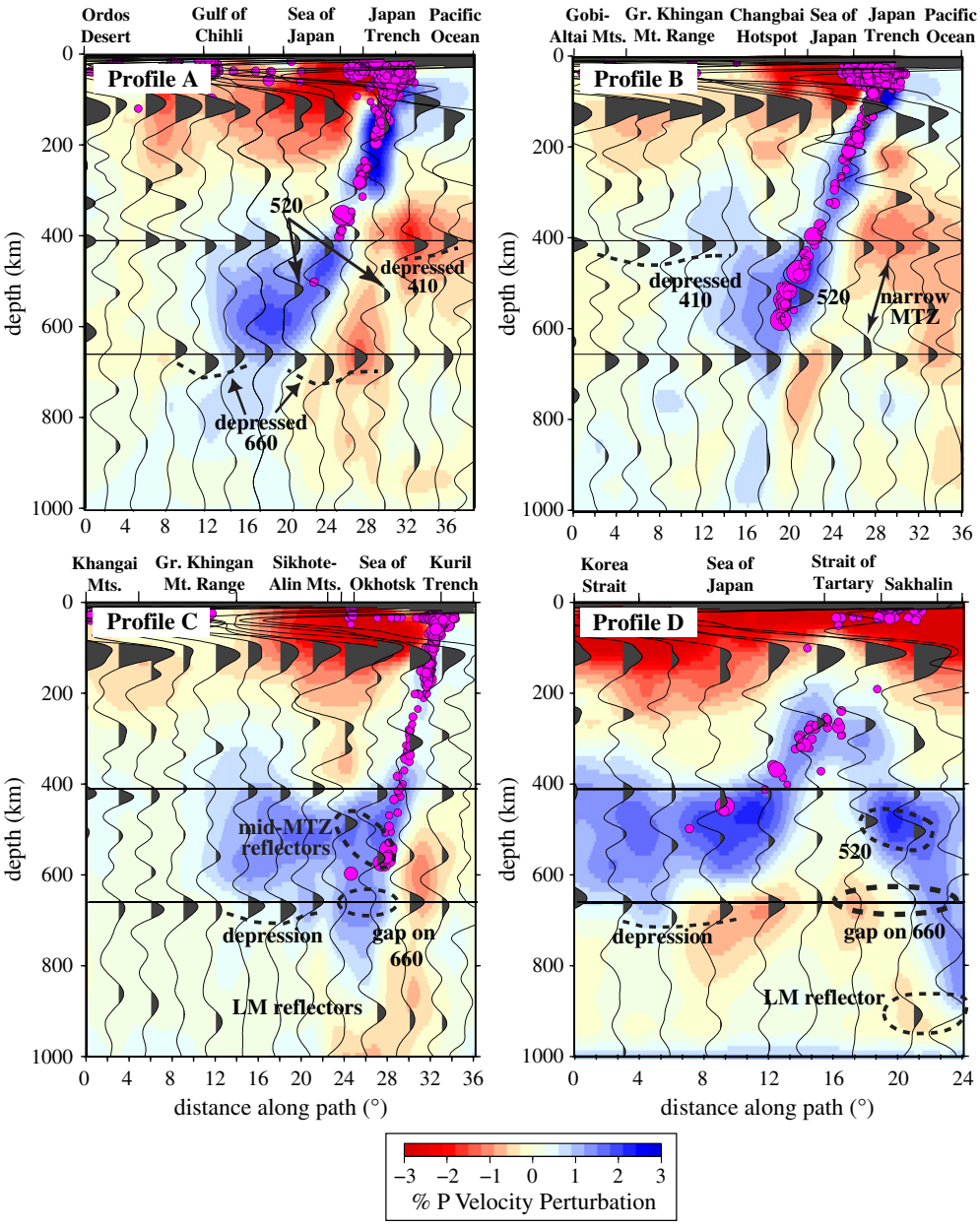

Fig. 4. Interpolated reflection stacks along Profiles A to D (see Fig. 2) superimposed on high-resolution *P*-wave velocities from Obayashi et al. (2006). The magenta circles show the earthquakes within the averaging window of each profile and the sizes of the circles scale with event magnitudes. Seismic activity extends down to 650 km and outlines the Wadati–Benioff zone in the northwestern Pacific region. Key observations are encircled or highlighted by dotted lines and arrows.

confined to the MTZ. Despite slightly reduced amplitudes, the MTZ phase boundaries are laterally continuous and the base of the MTZ between Korea Strait and Sea of Japan shows 30+ km depressions relative to the global average. Across southern Kuril arc, however, the amplitude of the 660 falls below noise level within a localized lower mantle high-velocity zone. As suggested by Profile C, the base of the northward dipping high-velocity structure partially overlaps with a strong reflector at 900–930 km depths (see Fig. 4, Profile D).

A common link between Japan and Kuril subduction zones is the presence of reflectors within the MTZ (see Figs. 3B and 4). We identify a single HRZ with maximum amplitudes in excess of 6% at ~525 km within the Wadati–Benioff zones in the two southern profiles. Two distinct reflectors are further detected across southern Kuril arc in the depth ranges of 500–530 km and 580–600 km (see Fig. 4D), and their amplitudes increase in the northward direction.

4. Discussion and interpretations

The effectiveness of *SS* precursors in resolving local or regional length-scale structures has been underscored by recent studies of subduction zones (Heit et al., 2010; Schmerr and Garnero, 2007), hot mantle plumes (Cao et al., 2011; Gu et al., 2009; Schmerr and Garnero, 2006) and crust (Rychert and Shearer, 2009). Despite concerns over Fresnel zone size and shape (Chaljub and Tarantola, 1997; Neele et al., 1997), shear waves such as *SS* precursors are capable of recovering structures at length scales beyond their 'nominal' resolution, especially when waveform information is incorporated (Ji and Nataf, 1998; Mégnin and Romanowicz, 2000). Major HRZs reported in this study are minimally affected by moderate changes to the CMP sizes and shapes. For example, the semi-linear structure across northern Honshu Islands and large lateral-scale depressions west of the Hokkaido Corner are consistently captured by reflection

maps constructed based on CMP areas of 12 deg^2 and 50 deg^2 (Fig. 5), despite instabilities associated with limited data traces in smaller CMPs (Fig. 5A) and over-smoothing in the case of larger averaging areas (Fig. 5B). Our heuristically determined averaging area of 24 deg^2 represents a reasonable compromise between image stability and resolution.

4.1. Average reflection amplitudes

The detectable ranges of amplitudes are 4–9% for *S410S* and 4–12% for *S660S*. The former range overlaps with the predicted values of ~8% from PREM (Dziewonski and Anderson, 1981) and the global average of 6.7% from *SS* precursors (Shearer, 1996), but the latter range falls well short of 14% based on PREM (Shearer, 2000). These individual amplitude estimates are strongly affected by the strength of *SS*, the normalizing reference phase. For instance, the presence of attenuating low-velocity structures (e.g. Huang and Zhao, 2006; Lei and Zhao, 2005; Zhao, 2001; Zhao et al., 1992, 2007), especially near back arc regions (e.g., Roth et al., 1999, 2000; Xu and Wiens, 1997; Zhao, 2001), could diminish *SS* and increase the relative amplitude of *SdS*. Compositional variations associated with Al at the base of upper mantle (Deuss, 2009; Deuss and Woodhouse, 2002; Weidner and Wang, 1998, 2000) or Fe content (Agee, 1998; Akaogi et al., 2007; Inoue et al., 2010) are also known to broaden phase boundary widths and reduce precursor amplitudes. A more stable parameter is the amplitude ratio between the 410 and the 660 (e.g., Shearer, 2000), which we estimate to be within the range of 0.7–0.8. This value is slightly higher than the earlier estimates of 0.64–0.68 based on global *SS* precursors (Shearer, 1996) and regional *ScS* observations (Revenaugh and Jordan, 1991), though it is in poor agreement with that of PREM (0.5). A regionally sharp 410 (Ai and Zheng, 2003; Benz and Vidale, 1993; Jasbinsek et al., 2010; Melbourne and Helmberger, 1998; Neele, 1996; Vidale et al., 1995) is possible but requires a quantitative analysis of the waveforms, particularly those prior to phase equalization. Additionally, since the average observed topography on the 660 is 25–30% larger relative to the 410 (see Figs. 3 and 4), defocusing and energy loss due to incoherent stacking (Shearer, 2000) would be more severe for reflections from the 660.

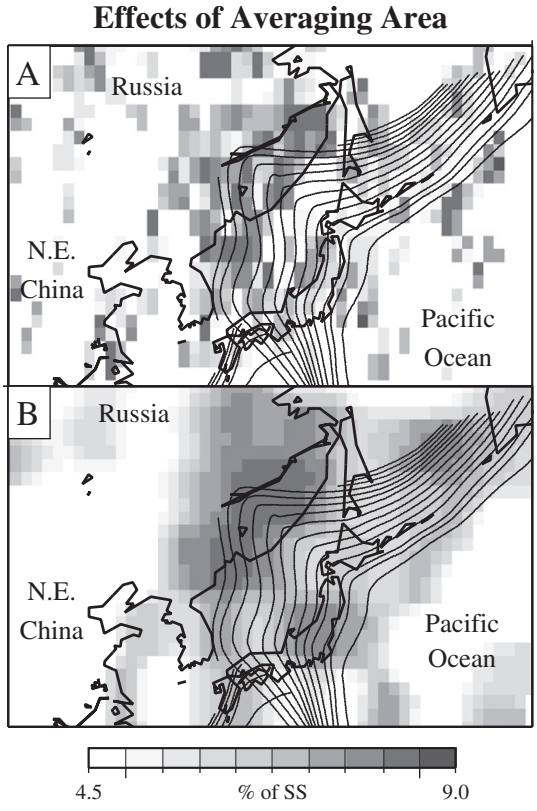

Fig. 5. A comparison of depth-converted reflection amplitudes at 680-km depth based on averaging CMP gathers of A) $2\times6=12$ deg^2, and B) $5\times10=50$ deg^2. The numbers on the left side of the equations are the dimensions (in arc deg) of the CMP gathers along section-parallel and section-perpendicular directions, respectively. The right side of the equation indicates the uniform CMP area for each experiment. Significant scatter in Fig. 5A suggests instability associated with limited numbers of traces in some CMP gathers, while the results in Fig. 5B suffers from over-smoothing. The main reflective structures such as strong depressions near the deepest part of the Wadati–Benioff zone are consistent between these maps.

4.2. Depth correlation of the 410 and 660

The depth-converted reflectivity profiles of this study offer new insights on the effect of mantle temperatures on the phase transition depths. For olivine-rich mantle compositions, the depths of the 410 and 660 should anticorrelate based on results of high-pressure laboratory experiments (e.g., Akaogi et al., 2007; Helffrich, 2000; Irifune et al., 1998; Ita and Stixrude, 1992; Katsura and Ito, 1989) as well as high-frequency seismic observations in the northwestern Pacific region (e.g., Ai and Zheng, 2003; Collier et al., 2001; Li et al., 2000; Ramesh et al., 2005; Saita et al., 2002; Tonegawa et al., 2006; van der Meijde et al., 2005). However, global surveys of the spectral contents and amplitudes of these two phase boundaries have often attributed a locally thick MTZ to a highly deformed 660 at the base of the upper mantle (Flanagan and Shearer, 1998; Gu and Dziewonski, 2002; Gu et al., 1998, 2003; Houser et al., 2008). The depth of the 410 remains problematic in view of expected phase boundary behavior (e.g., Deuss, 2007; Du et al., 2006; Fee and Dueker, 2004; Gilbert et al., 2003; Gu and Dziewonski, 2002; Gu et al., 2003; Schmerr and Garnero, 2007; Tauzin et al., 2008) and prompted additional assumptions involving MTZ velocity corrections (Deuss, 2007; Flanagan and Shearer, 1998; Gu et al., 2003; Houser et al., 2008; Schmerr and Garnero, 2006) and/or mechanisms predicated on extensive compositional variations (Deuss, 2007; Gu et al., 2009; Houser and Williams, 2010; Schmerr and Garnero, 2007).

Our migration results enable a careful examination of the correlation between temperature and discontinuity topography in the northwestern Pacific region. An excellent test case is Profile A in which both discontinuities are laterally continuous and exhibit strong topography (Fig. 6). The peak-to-peak depth variations of the 410 and 660 are approximately 30 km and 40 km, respectively, both exhibiting large deformation from the trench onset to the deepest part of the Wadati–Benioff zone across southern Japan (Fig. 6A). A simple bin-to-bin correlation, which implicitly assumes vertical continuity of seismic velocities, yields a small positive correlation. To account for non-vertical structures following the slab dip (~30°, Gudmundsson and Sambridge, 1998), we revise the correlation analysis by introducing an offset such that the depth of the 410 at a given location is correlated with that of the 660 at a location ~200 km further inland. The 'dip-corrected' phase boundaries show a clear negative correlation in the vicinity of the slab (see Fig. 6A) that favors a thermal origin for the observed shape of the MTZ. The negative correlation benefits from an anomalously shallow 410 within the Wadati–Benioff zone, which is a notable departure from earlier findings of global time-domain analyses of *SS* precursors (e.g., Flanagan and Shearer, 1998; Gu et al., 2003).

4.3. Continuity of the 410

There have been considerable discussions of the existence of, and support for, a water/melt rich layer near the top of the MTZ (Frost and Dolejs, 2007; Inoue et al., 1995, 2010; Kohlstedt et al., 1996; Smyth and Frost, 2001; Wood, 1995). Wadsleyite has a strong capacity to accommodate hydroxyl (OH^-) and can store up to 3 wt.% H_2O

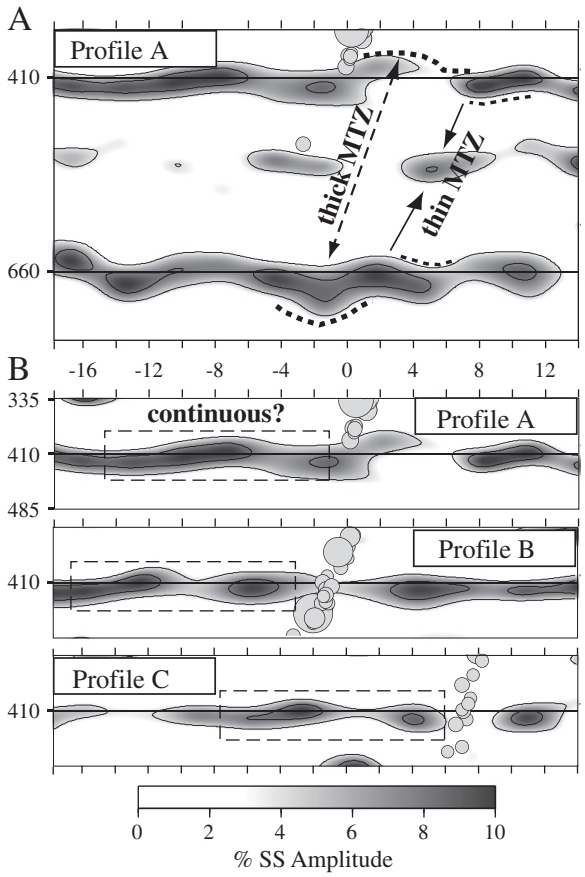

Fig. 6. (A) A subsection of the migrated reflectivity along Profile A. The gray circles mark the locations and sizes of deep earthquakes along the profile (see Fig. 4 for details). The contours superimposed on the shaded reflection amplitudes are taken at 4% and 8% values. (B) Magnified subsections of reflection amplitude near the top of the MTZ for all three profiles. The highlighted region shows a relatively continuous 410 above the stagnant part of Honshu slab.

under equilibrium conditions (Frost and Dolejs, 2007; Inoue et al., 1995, 2010; Wood, 1995). These laboratory-based measurements have been supported by regional (e.g., Revenaugh and Sipkin, 1994; Schaeffer and Bostock, 2010; Schmerr and Garnero, 2007; Zheng et al., 2007) and global (Deuss, 2009; Gu et al., 2009; Tauzin et al., 2010) seismic observations that require explanations beyond temperature. Mechanisms involving the infiltration of hydrous melt are elucidated further by geodynamical calculations and syntheses (e.g., Bercovici and Karato, 2003; Billen, 2008; Karato, 2006; Leahy and Bercovici, 2007, 2010).

Our migrated reflectivity structures provide further constraints on this hypothesized hydrous layer. The 410 west of the Wadati–Benioff zone (Fig. 6B) is consistently shallower than the regional average in this study. The largest topography is observed in the southernmost cross-section, reaching a depth of ~400 km beneath Korea and northeastern China. The two northern profiles B and C show modest highs of ~410 km near Great Khingan Range and Sikhote-Alin Mountains, respectively, and the average amplitudes of the 410 in all three profiles well exceed the regional averages (see Fig. 6B). These characteristics are reminiscent of those reported beneath Tonga subduction zone (Zheng et al., 2007) where a hydrous layer is suggested to reside atop the 410. While the highlighted region (see Fig. 6B) is farther away from the Wadati–Benioff zone than the target area in Zheng et al. (2007), metasomatism involving slab-derived fluids rising through the flattened part of slabs (Fukao et al., 2001, 2009; Zheng et al., 2007) could give rise to intraplate volcanoes near Changbai Mountain and Wudalianchi (Huang and Zhao, 2006; Lei and Zhao, 2005; Zhao, 2001; Zou et al., 2008).

Based on multiple cross-sections in South America, Schmerr and Garnero (2007) inferred a 'melt lens' from evidence of delayed and split/missing *S410S* east of the Nasca-South America convergent zone. A wide 410 reflection gap is corroborated by Contenti et al. (2012) based on *SS* precursors and the same imaging technique presented in this study, but the associated *S410S* waveforms from South America are much more complex than those shown in this study. If a fluid-rich layer exists atop the MTZ, its spatial scale, infiltration/storage mechanism and/or chemistry (e.g., Richard and Iwamori, 2010) beneath the Pacific Northwest would most likely differ from those beneath Tonga and South America.

4.4. Slab stagnation and distortion

Subducted ocean basins in the western Pacific region have been known to deflect to a near-horizontal direction at the MTZ for nearly two decades (Fukao et al., 1992; Okino et al., 1989; van der Hilst et al., 1991). Since these early reports, ample evidence of slab stagnation (Fukao et al., 1992, 2001) has been provided by global and regional tomographic images (Fukao et al., 2001, 2009; Li and van der Hilst, 2010; Sugioka et al., 2010; Zhao and Ohtani, 2009), as well as by anomalous dip-angle variations in the distribution of intermediate-depth earthquakes (Chen et al., 2004). The conditions and characteristics of stagnant slabs were constrained further by recent numerical calculations that incorporated thermo-petrological buoyancy forces (Bina and Kawakatsu, 2010; Bina et al., 2001; Tetzlaff and Schmeling, 2000), rheology (Billen, 2008, 2010; Billen and Hirth, 2007) and plate history and rollback (Christensen, 2010; Nakakuki et al., 2010; Tagawa et al., 2007; Torii and Yoshioka, 2007; Zhu et al., 2010).

With the help of seismic velocities, the reflectivity information provided by our study can place crucial constraints on slab deformation at the base of the MTZ and the shallow lower mantle. Our observations suggest reduced topography on the 660 in the northward direction (see Profiles A and B in Fig. 4), which is consistent with earlier findings based on receiver functions (Niu et al., 2005) and postcursors of *sScS* (Yamada et al., 2009). A 'soft' slab under the influence of trench migration and rollback may be possible beneath northern Honshu arc (Li et al., 2008). However, for the same region Li et al. (2008) detected little or no oceanward broadening of the 660 from high-resolution *S* to *P* converted waves. This result is inconsistent with the observed shift in this study between the high-velocity zone and the onset of the broad depression in the vicinity of the island arcs (see Figs. 4 and 6A). While resolution differences between *SS* precursors and receiver functions may play a role, the 100–300 km horizontal broadening of the 660 in the oceanward direction could be caused by slab 'pile-ups' at the base of MTZ.

A more intriguing observation from the two southern profiles is two distinct zones of large lateral scale depression: 1) near the piercing point of the slab at the base of MTZ, and 2) in the western half of the stagnant slab (e.g., Fukao et al., 2009; Huang and Zhao, 2006). These two basins are nearly identical in shape, and the depth of the 660 between them is raised sharply to 655–660 km. By assuming a reference discontinuity depth of 670 km, we estimate the horizontal dimensions of the depression zones (Seg 1 and Seg 3) to be 350–450 km in Profile A (Fig. 7A) and 550–600 km in Profile B (Fig. 7B). The respective phase boundary elevations between the basins are roughly estimated to be ~600 km and ~350 km, rendering a total length of ~950 km (i.e., Seg 2 + Seg 3) for both profiles beyond the slab piercing point at the 660. This value falls within an estimated length of 800–1000 km for deflected slabs (Fukao et al., 2009; Huang and Zhao, 2006), though true length could be slightly smaller due to the effect of spatial averaging. The flat part of the slab, which is expected to reside on the 660, is no wider than 600 km.

The shape of the 660 raises new questions about the 'flatness' (Okino et al., 1989) of stagnant slabs. The observation of contention

is the average or shallow 660 between the two distinct basins, which implies a significant temperature/compositional gradient leading to the center of the stagnating slab segment. This observation is inconsistent with the broad depressions reported earlier based on seismic tomography (see Fukao et al., 2009 and references therein) and reflection depth/MTZ thickness imaging (e.g., Flanagan and Shearer, 1998; Gu et al., 1998, 2003; Houser et al., 2008; Lawrence and Shearer, 2006; Shearer and Masters, 1992). The amplitude of the 660 within this uplifted region (see Seg 3, Fig. 7A and B) is higher than the regional averages, which may be interpreted as a narrow ringwoodite to perovskite + magnisiowustite phase loop at temperatures above the geotherm. Formations of twin basins on the 660 are plausible according to geodynamical calculations of slab geometry that incorporated trench retreat (Christensen, 1996; Tagawa et al. 2007; Zhu et al., 2010) or temperature- and pressure-dependent viscosity (see Fig. 12 of Fukao et al., 2009; Karato and Wu, 1993). These calculations suggest a deep 660 at the slab piercing and MTZ re-entry points, between which the phase boundary remains nearly unperturbed (see Fig. 7A). While the horizontally oriented, lower-mantle slab segment in Fig. 7A (e.g., Christensen, 1996; Fukao et al., 2009; Tagawa et al., 2007) is not convincingly supported by our *SS* precursor observations, buckling (Bagly, 1982; Ribe et al., 2007) is plausible due to interactions between the tip of the descending slab and the viscous lower mantle (e.g., Kellogg et al., 1999; Obayashi et al., 2006). During these episodes, entrapped ambient mantle material could form isolated, higher-temperature pockets within a highly deformed stagnant slab. Trench migration and rollback history (Christensen, 1996; see Schmid et al., 2002 for the case of Farallon plate subduction), water (e.g., Huang and Zhao, 2006; Inoue et al., 1995, 2010; Kohlstedt et al., 1996; Litasov et al., 2006; Ohtani et al., 2001; Suetsugu et al., 2006; van der Meijde et al., 2003), grain-size reduction (e.g., Billen, 2010; Nakakuki et al., 2010), and possible separation of oceanic crust from the descending lithosphere (Hirose et al., 1999, 2005; Irifune and Ringwood, 1993; van Keken et al., 1996) could all contribute large internal gradients on the 660 within the 'flat' part of the slab.

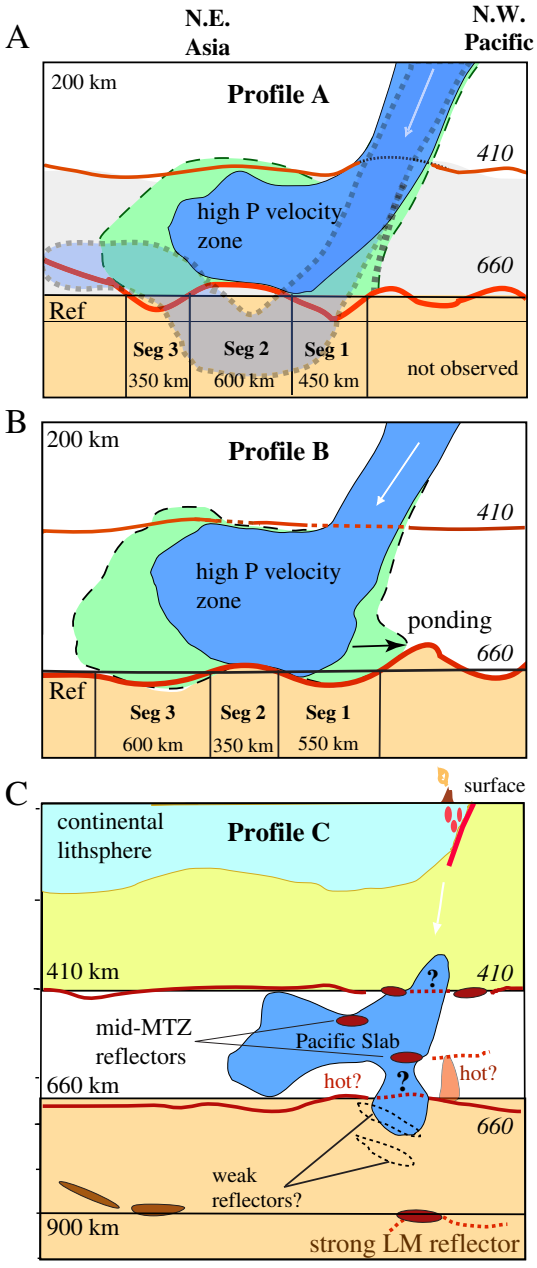

Fig. 7. The observed depths of the 410 and 660 beneath Profiles A–C with interpretations. The undulations on the 410 and 660 have been exaggerated by a factor of 2 from the original observations presented in Fig. 4. The short dashed lines mark regions of low reflection amplitude and the white arrows indicate the dip of the Wadati–Benioff zones. The region shaded in blue shows 1% *P* velocity perturbations from Obayashi et al. (2006)), and the regions shaded in green (see Profiles A and B) represent interpreted MTZ low-temperature regimes based on the observed *SS* precursor amplitudes of this study. Three distinct sub-regions at the base of the upper mantle are labeled Seg 1–3. Their dimensions are estimated based on a reference depth of 670 km and rounded to the nearest 50 km. In Fig. 7A, the region shaded in gray shows the shape of a stagnant slab from recent numerical simulations that consider temperature- and pressure-dependent viscosity (edited from Fig. 12 of Fukao et al., 2009 and Fig. 4 of Nakakuki et al., 2010).

4.5. Slab penetration beneath southern Kuril arc

The reflectivity structures shed new light on the long-standing debate about the depth of slab in the Pacific Northwest (Fukao et al., 1992; Fukao et al., 2001, 2009; van der Hilst et al., 1991; van der Hilst et al., 1997). While the vertical extent of slabs and the general style of mantle convection remain debated on the global scale, there is growing evidence of scattered and deformed slab material in the lower mantle (Bijwaard et al., 1998; Chang et al., 2010; Courtier and Revenaugh, 2008; Fukao et al., 2001, 2009; Li and van der Hilst, 2010; Obayashi et al., 2006; van der Hilst et al., 1997).

Among the various HRZs documented in this study, sub-MTZ anomalies in Profiles C and D present the best arguments for slab penetration into the lower mantle. The most visible change from central Honshu to southern Kuril arcs is the reflection amplitude reduction of both the 410 and the 660, highlighted by apparent reflection gaps in the northernmost transect. These gaps coincide with the Wadati–Benioff zone of the Kuril slab (Fig. 7C) and their origins remain enigmatic. For instance, increasing Al content could broaden the depth range of garnet-to-perovskite transformation and influence olivine and pyroxene normative proportions near the base of the upper mantle (Gasparik, 1996; Weidner and Wang, 1998). This scenario is plausible when majorite garnet transforms to metastable ilminite and, eventually, to Ca-perovskite (e.g., Weidner and Wang, 1998, 2000) in subduction zones. The presence of Al-bearing akimotoite could introduce further complexities, such as a high velocity layer or a steep velocity gradient, to mid MTZ depths at low temperatures (Gasparik, 1996; Wang et al., 2004). However, changes in Al content mainly impact mantle reflectivity structure under mid-to-lower MTZ pressure-temperature conditions (e.g., Tateno et al., 2005; Wang et al., 2004; Weidner and Wang, 2000), which fails to explain the weak 410 within the Kuril slab (see Fig. 4, Profile C and Fig. 7C). Alternatively, increasing Fe concentration could substantially broaden the phase loops of both olivine-wadsleyite and ringwoodite to perovskite + magnisiowustite transitions (Akaogi et al., 2007; Fiorenza et al., 2011; Inoue et al., 2010; Litasov et al., 2006), thus

reducing the reflection amplitudes of both discontinuities. Observational support for Fe enrichment in subduction zones (Agee, 1998; Deon et al., 2011) remains insufficient.

Water transported into the MTZ by slabs could potentially modify the impedance contrast, hence the visibility of a reflecting body (Fukao et al., 2009; Ichiki et al., 2006; Ohtani and Sakai, 2008; van der Meijde et al., 2003). Aided by the strong inclinations of wadsleyite and ringwoodite to retain water (Bercovici and Karato, 2003; Inoue et al., 1995; Kohlstedt et al., 1996; see Fukao et al., 2009 for review), a hydrous MTZ can simultaneously affect the width and depth of the 660 (Akaogi et al., 2007; Inoue et al., 2010; Litasov et al., 2006). Effect of water on the phase loop of olivine-Wadsleyite transition is, unfortunately, both complex and weaker than expected based on 1 wt.% H_2O inclusion (Inoue et al., 2010). A larger amount of water is likely required within the descending slab to diminish the amplitude of *S410S* beyond the detection threshold. Recent seismic observations (Bina and Kawakatsu, 2010; Fukao et al., 2009; Suetsugu et al., 2006, 2010) have generally favored 'dry' (e.g., <0.5 wt.% H_2O, Suetsugu et al., 2006, 2010) slabs in various subduction zones along the western Pacific plate boundaries, however. In addition, the 660 appears to be locally elevated, despite a diminutive amplitude, which is at odds with the expected effect of water in the MTZ (Billen, 2008; Litasov et al., 2006).

Aside from minerological explanations, the observed reflection gaps are most definitely affected by wave optics. Similar to the scattering of light, the stacked amplitudes of the underside SH-wave reflections are sensitive to the geometry of the reflecting surface. For instance, a dipping structure or interface can easily cause defocusing or scattering, depending on the size of the structure relative to the wavelength of the incoming wave (Chaljub and Tarantola, 1997). Deconstructive wave field interference from multiple reflectors could further reduce the perceived strength of the 660. Within low-temperature slabs, garnet–ilmenite–perovskite transitions (e.g., Akaogi et al., 2002; Vacher et al., 1998; Weidner and Wang, 1998, 2000) have been suggested to take place over a depth range of 60–100 km at the base of the MTZ (Akaogi et al., 2002; Vacher et al., 1998). Observationally, multiple reflectors have been reported under different tectonic settings (e.g., Ai and Zheng, 2003; Deuss and Woodhouse, 2002; Schmerr and Thomas, 2011; Tibi et al., 2007), but remain questionable beneath the western Pacific region (Lebedev et al., 2002; Niu et al., 2005; Tonegawa et al., 2006). In this study, only the Kuril profile (see Fig. 4C, D) hinted at subtle reflectors with 4–5% amplitudes at ~700- and 780-km depths along slab dip (see Fig. 7C).

The presence of a robust lower-mantle HRZ beneath Kuril slab (see Fig. 7C) lends further support for a deep Kuril slab. Phase transitions of Ca-perovskite (Stixrude et al., 2007), metastable garnet (Kawakatsu and Niu, 1994; Kubo et al., 2002), stishovite (Hirose et al., 2005; Ohtani, 2005), as well as transformations of dense hydrous magnesium silicates under lower-mantle pressure–temperature conditions (Ohtani, 2005; Ohtani et al., 2001; Richard et al., 2006; Shieh et al., 1998 and references therein), are possible origins of the observed lower-mantle reflectors (e.g., Kaneshima and Helfrich, 1999, 2003; Niu et al., 2003). A slightly weaker lower-mantle HRZ in the depth range of 850–1000 km away from active subduction (see Fig. 4A and 7C) remains enigmatic.

4.6. Other HRZs and their potential origins

Two additional reflection signals from this study could have significant implications if confirmed. First, we identify one (across Honshu arc) or more (across southern Kuril arc) reflectors with amplitudes ranging from 5% to 9% within the MTZ (see Fig. 3B, 4 and 7). The peak locations generally reside within the descending slab, with the notable exception of a strong 520 east of the Wadati-Benioff zone beneath central Honshu island (see Fig. 3A) The origins of MTZ reflective structures or velocity gradients remain controversial, though their existence has long been documented in the study region based on travel times (Fukao, 1977). It was later proposed to be a weak global seismic discontinuity from studies of *SS* precursors (Shearer, 1990, 1991), despite suggestions of artifacts associated with low-frequency side-lobes of *S410S* and *S660S* (Bock, 1994). Highly undulating MTZ reflectors received further support from reflected and converted body waves (Chevrot et al., 1999; Deuss, 2009; Deuss and Woodhouse, 2002; Flanagan and Shearer, 1998; Gossler and Kind, 1996; Gu et al., 1998; Gu et al., 2003; Lawrence and Shearer, 2006; Shearer, 1996; Shen et al., 2008), and were generally attributed to wadsleyite to ringwoodite (Bina, 2003; Helffrich, 2000) and garnet to Ca-perovskite (Ita and Stixrude, 1992) phase changes. Within subduction zones, these two transformations likely occur at different MTZ depths (Saikia et al., 2008) and manifest into distinct reflectors (Deuss, 2009; Deuss and Woodhouse, 2002) resembling those detected below southern Kuril arc in this study. Alternative explanations include a delayed meta-stable olivine phase transition (Bina and Kawakatsu;, 2010; Iidaka and Suetsugu, 1992; Jiang et al., 2008; Sung and Burns, 1976), water within slabs (e.g., Inoue et al., 1995, 2010; Koyama et al., 2006; Lawrence and Wysession, 2006) and a flat garnetite layer (Shen et al., 2008). A combination of these mechanisms may be responsible for the different signatures in the Honshu (a single 520 reflector) and Kuril (multiple MTZ reflectors) profiles.

Finally, a narrow MTZ and a series of strong HRZs (see Figs. 4 and 7) suggest reduced MTZ temperatures east of the Wadati–Benioff zone. This interpretation is supported by recent studies of *ScS* reverberations (Bagley et al., 2009; Revenaugh and Sipkin, 1994), seismic tomography (Huang and Zhao, 2006; Obayashi et al., 2006; Zhao and Ohtani, 2009), and electrical conductivity (Ichiki et al., 2006). The large reflection amplitudes of these reflections (8–12% of *SS*) likely require compositional variations associated with a residual thermal plume from the past 130 Ma (Honda et al., 2007; Ichiki et al., 2006; Miyashiro, 1986; Obayashi et al., 2006; Zhao and Ohtani, 2009; Zou et al., 2008).

5. Conclusions

Key conclusions from our study of SS precursors sampling the northwestern Pacific subduction zones are:

1. The depths of the 410 and 660 are negatively correlated if slab dip is considered, especially beneath central Honshu arc. The MTZ olivine phase boundary variations are mainly governed by temperature.
2. The Pacific plate stagnates across central Honshu island at MTZ depths, but the center of the stagnant slab appears to be strongly deformed or buckled near the base of the upper mantle, i.e., the stagnant slab may not be as flat as previously suggested. Eastward broadening of the 660 is likely due to slab 'pile-ups'.
3. The Pacific plate extends below the transition zone across southern Kuril arc. Major mass and heat fluxes and possible compositional variations are expected near the slab piercing point.
4. Strong reflectors exist within/near the descending slabs at mid MTZ and lower mantle depths.

From a technical standpoint, the results presented in this study provide a glimpse of the future for regional-scale analysis based on intermediate-period *SS* precursors. Increasingly diverse applications in recent years have underlined the remarkable resolving power of this data set, one that was traditionally tapped as a 'low resolution' constraint on mantle structure. This trend will continue in the foreseeable future, especially in view of the growing number of global seismic networks and applications of array methods.

Supplementary data related to this article can be found online at 10.1016/j.epsl.2012.03.023

Acknowledgments

We thank Peter Shearer for constructive suggestions and extraordinary professionalism in handling this manuscript. This study also benefited from insightful reviews by Nicholas Schmerr and an anonymous reviewer, as well as from the technical assistance of IRIS Data Management Center. National Science and Engineering Council (NSERC) and the University of Alberta provided funding support for this research project.

References

Agee, C.B., 1998. Phase transformations and seismic structure in the upper mantle and transition zone. Rev. Mineralog. Geochem. 37, 165–203.
Ai, Y., Zheng, T., 2003. The upper mantle discontinuity structure beneath eastern China. Geophys. Res. Lett. 30. doi:10.1029/2003GL017678.
Akaogi, M., Tanaka, A., Ito, E., 2002. Garnet–ilmenite–perovskite transitions in the system $Mg_4Si_4O_{12}$–$Mg_3Al_2Si_3O_{12}$ at high pressures and high temperatures: phase equilibria, calorimetry and implications for the mantle structure. Phys. Earth Planet. Inter. 132, 303–324.
Akaogi, M., Takayama, H., Kojitani, H., Kawaji, H., Atake, T., 2007. Low-temperature heat capacities, entropies and enthalpies of Mg_2SiO_4 polymorphs, and α–β–γ and post-spinel phase relations at high pressure. Phys. Chem. Miner. 34, 169–183.
An, Y., Gu, Y.J., Sacchi, M., 2007. Imaging mantle discontinuities using least-squares Radon transform. J. Geophys. Res. 112. doi:10.1029/2007JB005009.
An, M., Feng, M., Zhao, Y., 2009. Destruction of lithosphere within the north China craton inferred from surface wave tomography. Geochem. Geophys. Geosyst. 10, Q08016. doi:10.1029/2009GC002562.
Bagley, B., Courtier, A.M., Revenaugh, J., 2009. Melting in the deep upper mantle oceanward of the Honshu slab. Phys. Earth Planet. Inter. 175, 137–144.
Bagly, B., 1982. Geometry of subducted plates and island arcs viewed as a buckling problem. Geology 10, 629–632.
Bassin, C., Laske, G., Masters, G., 2000. The current limits of resolution for surface wave tomography in North America. EOS Trans. Am. Geophys. Union 81, F897.
Benz, H.M., Vidale, J.E., 1993. Sharpness of upper-mantle discontinuities determined from high-frequency reflections. Nature 365, 147–150.
Bercovici, D., Karato, S., 2003. Whole mantle convection and the transition-zone water filter. Nature 425, 39–44.
Bijwaard, H., Spakman, W., Engdahl, E.R., 1998. Closing the gap between regional and global travel time tomography. J. Geophys. Res. 103, 30055–30078.
Billen, M.I., 2008. Modeling the dynamics of subducting slabs. Annu. Rev. Earth Planet. Sci. 36, 325–356.
Billen, M.I., 2010. Slab dynamics in the transition zone. Phys. Earth Planet. Inter. 183, 296–308.
Billen, M.I., Hirth, G., 2007. Rheologic controls on slab dynamics. Geophys. Geochem. Geosystems 8, Q08012. doi:10.1029/2007GC001597.
Bina, C.R., 2003. In: Carson, R. (Ed.), Seismological constraints upon mantle composition. : Treatise on Geochemistry, 2. Elsevier Science Publishing, Oxford, pp. 39–59.
Bina, C.R., Kawakatsu, H., 2010. Buoyancy, bending and seismic visibility in deep slab stagnation. Phys. Earth Planet. Inter. 183, 330–340.
Bina, C.R., Stein, S., Marton, F.C., Van Ark, E.M., 2001. Implications of slab mineralogy for subduction dynamics. Phys. Earth Planet. Inter. 127, 51–66.
Bird, P., 2003. An updated digital model of plate boundaries. Geochem. Geophys. Geosyst. 4, 1027.
Bock, G., 1994. Synthetic seismogram images of upper mantle structure: no evidence for a 520-km discontinuity. J. Geophys. Res. 99, 15843–15851.
Cao, Q., Van der Hilst, R.D., De Hoop, M.V., Shim, S.-H., 2011. Seismic imaging of transition zone discontinuities suggests hot mantle west of Hawaii. Science 332, 1068–1071. doi:10.1126/science.1202731.
Chaljub, E., Tarantola, A., 1997. Sensitivity of *SS* precursors to topography on the upper-mantle 660-km discontinuity. Geophys. Res. Lett. 24, 2613–2616.
Chang, S.-J., van der Lee, S., Flanagan, M.P., Bedle, H., Marone, F., Matzel, E.M., Pasyanos, M.E., Rodgers, A.J., Romanowicz, B., Schmid, C., 2010. Joint inversion for 3-dimensional S-velocity mantle structure along Tethyan margin. J. Geophys. Res. 115, B08309. doi:10.1029/2009JB007204.
Chen, P., Bina, C.R., Okal, E.A., 2004. A global survey of stress orientations in subducting slabs as revealed by intermediate-depth earthquakes. Geophys. J. Int. 159, 721–733.
Chevrot, S., Vinnik, L., Montagner, J.-P., 1999. Global-scale analysis of the mantle Pds phases. J. Geophys. Res. 104 20,203–20,220, doi:10.1029/1999JB900087.
Christensen, U., 1995. Effects of phase transitions on mantle convection. Annu. Rev. Earth Planet. Sci. 23, 65–87.
Christensen, U.R., 1996. The influence of trench migration on slab penetration into the lower mantle. Earth Planet. Sci. Lett. 140, 27–39.
Christensen, U., 2010. Geodynamic models of deep subduction. Phys. Earth Planet. Inter. 127, 25–34.
Collier, J., Helffrich, G., Wood, B., 2001. Seismic discontinuities in subduction zones. Phys. Earth Planet. Inter. 127, 39–49.
Contenti, S., Gu, Y.J., Okeler, A., Sacchi, M., 2012. Shear wave reflectivity imaging of the Nazca-South America subduction zone: Stagnant slab in the mantle transition zone? Geophys. Res. Lett. 39, L02310. doi:10.1029/2011GL050064.
Courtier, A.M., Revenaugh, J., 2008. Slabs and shear wave reflectors in the mid-mantle. J. Geophys. Res. 113, B08312. doi:10.1029/2007JB005261.
DeMets, C., Gordon, R.G., Argus, D.F., Stein, S., 1990. Current plate motions. Geophys. J. Int. 101, 425–478.
Deon, F., Koch-Mueller, M., Rhede, D., Wirth, W., 2011. Water and iron effect on the P-T-x coordinates of the 410-km discontinuity in the Earth upper mantle. Contributions to Mineral. Petrol. 161, 653–666.
Deuss, A., 2007. Seismic observations of transition zone discontinuities beneath hotspot location. In: Foulger, G.R., Jurdy, D.M. (Eds.), Plates, Plumes and Planetary Processes, pp. 121–136.
Deuss, A., 2009. Global observations of mantle discontinuities using *SS* and PP precursors. Surv. Geophys. 30, 301–326.
Deuss, A., Woodhouse, J.H., 2002. A systematic search for mantle discontinuities using *SS*-precursors. Geophys. Res. Lett. 29, 1249–1252.
Du, Z., Vinnik, L.P., Foulger, G.R., 2006. Evidence from *P*-to-*S* mantle converted waves for a flat '660-km' discontinuity beneath Iceland. Earth Planet. Sci. Lett. 241, 271–280.
Duan, Y., Zhao, D., Zhang, X., et al., 2009. Seismic structure and origin of active intraplate volcanoes in Northeast Asia. Tectonophysics 470, 257–266.
Dziewonski, A.M., Anderson, D.L., 1981. Preliminary reference earth model. Phys. Earth Planet. Inter. 25, 297–356.
Dziewonski, A.M., Chou, T.A., Woodhouse, J.H., 1981. Determination of earthquake source parameters from waveform data for studies of global and regional seismicity. J. Geophys. Res. 86, 2825–2852.
Efron, B., 1977. Bootstrap method, another look at the Jackknife. Ann. Stat. 7, 1–26.
Fee, D., Dueker, K., 2004. Mantle transition zone topography and structure beneath the Yellowstone hotspot. Geophys. Res. Lett. 31, L18603. doi:10.1029/2004GL020636.
Feng, M., An, M., 2010. Lithospheric structure of the Chinese mainland determined from joint inversion of regional and teleseismic Rayleigh-wave group velocities. J. Geophys. Res. 115, B06317. doi:10.1029/2008JB005787.
Fiorenza, D., Koch-Mueller, M., Rhede, D., Wirth, R., 2011. Water and iron effect on the P–T–x coordinates of the 410-km discontinuity in the Earth upper mantle. Contrib. Miner. Petrol. 161, 653–666.
Flanagan, M.P., Shearer, P.M., 1998. Global mapping of topography on transition zone velocity discontinuities by stacking *SS* precursors. J. Geophys. Res. 103, 2673–2692.
Frost, D., Dolejs, D., 2007. Experimental determination of the effect of H_2O on the 410-km seismic discontinuity. Earth Planet. Sci. Lett. 256, 182–195.
Fukao, Y., 1977. Upper mantle P structure on the ocean side of the Japan-Kuril Arc. Geophys. J. R. Astron. Soc. 50, 621–642.
Fukao, Y., Obayashi, M., Inoue, H., Nenbai, M., 1992. Subducting slabs stagnant in the Mantle Transition Zone. J. Geophys. Res. 97, 4809–4822.
Fukao, Y., Widiyantoro, S., Obayashi, M., 2001. Stagnant slabs in the upper and lower mantle transition region. Rev. Geophys. 39, 291–323.
Fukao, Y., Obayashi, M., Nakakuki, T., Deep Slab Project Group, 2009. Stagnant slab: a review. Annu. Rev. Earth Planet. Sci. 37, 19–46.
Gasparik, T., 1996. Melting experiments on the enstatite–diopside join at 70–224 kbar, including the melting of diopside. Contrib. Mineralog. Petrol. 124, 139–153.
Gilbert, J.H., Sheehan, A.F., Dueker, K.G., Molnar, P., 2003. Receiver functions in the western United States, with implications for upper mantle structure and dynamics. J. Geophys. Res. 108, B5. doi:10.1029/2001JB001194.
Gorbatov, A., Kennett, B.L.N., 2002. Joint bulk-sound and shear tomography for western Pacific subduction zones. Earth Planet. Sci. Lett. 210, 527–543.
Gorbatov, A., Widiyantoro, S., Fukao, Y., Gordeev, E., 2000. Signature of remnant slabs in the North Pacific from P-wave tomography. Geophys. J. Int. 142, 27–36.
Gossler, J., Kind, R., 1996. Seismic evidence for very deep roots of continents. Earth Planet. Sci. Lett. 138, 1–13.
Grand, S.P., 2002. Mantle shear-wave tomography and the fate of subducted slabs. Philos. Trans. R. Soc. Lond. A 360, 2475–2491.
Gu, Y.J., Dziewonski, A.M., 2002. Global variability of transition zone thickness. J. Geophys. Res. 107 (B7), 2135. doi:10.1029/2001JB000489.
Gu, Y.J., Dziewonski, A.M., Agee, C.B., 1998. Global de-correlation of the topography of transition zone discontinuities. Earth Planet. Sci. Lett. 157, 57–67.
Gu, Y.J., Dziewonski, A.M., Ekström, G., 2003. Simultaneous inversion for mantle shear velocity and topography of transition zone discontinuities. Geophys. J. Int. 154, 559–583.
Gu, Y.J., Schultz, R., Okeler, A., 2008. Migration and radon imaging of the western Pacific subduction zones using SdS waves. EOS Trans. Am. Geophys. Union 89 DI12A-08.
Gu, Y.J., An, Y., Sacchi, M., Schultz, R., Ritsema, J., 2009. Mantle reflectivity structure beneath oceanic hotspots. Geophys. J. Int. doi:10.1111/j.1365-246X.2009.04042.x
Gudmundsson, O., Sambridge, M., 1998. A regionalized upper mantle (RUM) seismic model. J. Geophys. Res. 103, 7121–7136.
Heit, B., Yuan, X., Bianchi, M., Kind, R., Gossler, J., 2010. Study of the lithospheric and upper-mantle discontinuities beneath eastern Asia by *SS* precursors. Geophys. J. Int. 183, 252–266.
Helffrich, G., 2000. Topography of the transition zone seismic discontinuities. Rev. Geophys. 38, 141–158.
Hirose, K., Fei, Y., Ma, Y., Mao, H.K., 1999. The fate of subducted basaltic crust in the Earth's lower mantle. Nature 397, 53–56.
Hirose, K., Takafuji, N., Sata, N., Ohishi, Y., 2005. Phase transition and density of subducted MORB crust in the lower mantle. Earth Planet. Sci. Lett. 237, 239–251.
Honda, S., Morishige, M., Orihashi, Y., 2007. Sinking hot anomaly trapped at the 410 km discontinuity near the Honshu subduction zone, Japan. Earth Planet. Sci. Lett. 261, 565–577.
Houser, C., Williams, Q., 2010. Reconciling Pacific 410 and 660 km discontinuity topography, transition zone shear velocity patterns, and mantle phase transitions. Earth Planet. Sci. Lett. 296, 255–266.

Houser, C., Masters, G., Flanagan, M., Shearer, P., 2008. Determination and analysis of long-wavelength transition zone structure using *SS* precursors. Geophys. J. Int. 174, 178–194.
Huang, J., Zhao, D., 2006. High-resolution mantle tomography of China and surrounding regions. J. Geophys. Res. 111, B09305. doi:10.1029/2005JB004066.
Ichiki, M., Baba, K., Obayashi, M., Utada, H., 2006. Water content and geotherm in the upper mantle above the stagnant slab: interpretation of electrical conductivity and seismic P-wave velocity models. Phys. Earth Planet. Inter. 155, 1–15.
Iidaka, T., Suetsugu, D., 1992. Seismological evidence for metastable olivine inside a subducting slab. Nature 356, 593–595.
Inoue, T., Yurimoto, H., Kudoh, Y., 1995. Hydrous modified spinel, MgSiHO: a new water reservoir in the mantle transition region. Geophys. Res. Lett. 22, 117–120.
Inoue, T., Ueda, T., Tanimoto, Y., Yamada, A., Irifune, T., 2010. The effect of water on the high-pressure phase boundaries in the system Mg_2SiO_4–Fe_2SiO_4. J Phys. Conf. Series 215. doi:10.1088/1742-6596/215/1/012101.
Irifune, T., Ringwood, A.E., 1993. Phase transformations in subducted oceanic crust and buoyancy relationships at depths of 600–800 km in the mantle. Earth Planet. Sci. Lett. 117, 101–110.
Irifune, T., Nishiyama, N., Kuroda, K., Inoue, T., Isshiki, M., Utsumi, W., Funakoshi, K., Urakawa, S., Uchica, T., Katsura, T., Ohtaka, O., 1998. The postspinel phase boundary in Mg_2SiO_4 determined by in situ X-ray diffraction. Science 279, 1698–1700.
Ita, J., Stixrude, S., 1992. Petrology, elasticity, and composition of the mantle transition zone. J. Geophys. Res. 97, 6849–6866.
Jasbinsek, J.J., Dueker, K.G., Hansen, S.M., 2010. Characterizing the 410 km discontinuity low-velocity layer beneath the LA RISTRA array in the North American Southwest. Geochem. Geophys. Geosyst. 11, Q03008. doi:10.1029/2009GC002836.
Ji, Y., Nataf, H.C., 1998. Detection of mantle plumes in the lower mantle by diffraction tomography: Hawaii. Earth Planet. Sci. Lett. 159, 99–115.
Jiang, G., Zhao, D., Zhang, G., 2008. Seismic evidence for a metastable olivine wedge in the subducting Pacific slab under Japan Sea. Earth Planet. Sci. Lett. 270, 300–307.
Kaneshima, S., Helffrich, G., 1999. Dipping low-velocity layer in the midlower mantle: evidence for geochemical heterogeneity. Science 283, 1888–1891.
Kaneshima, S., Helfrich, G., 2003. Subparallel dipping heterogeneities in the mid lower mantle. J. Geophys. Res. 108. doi:10.1029/2001jb001596.
Kárason, H., van der Hilst, R.D., 2000. Constraints on mantle convection from seismic tomography. In: Richards, M.R., Gordon, R., van der Hilst, R.D. (Eds.), The history and dynamics of global plate motion. : Geophysical Monograph, 121. American Geophysical Union, Washington, D.C, pp. 277–288.
Karato, S., 2006. Remote sensing of hydrogen in the Earth's mantle. Rev. Mineralog. Geochem. 62, 343–375.
Karato, S., Wu, P., 1993. Rheology of the upper mantle: a synthesis. Science 260, 771–778.
Katsura, T., Ito, E., 1989. The system $Mg_2S_iO_4$–$Fe_2S_iO_4$ at high pressures and temperatures; precise determination of stabilities of olivine, modified spinel, and spinel. J. Geophys. Res. 94, 15663–15670.
Kawakatsu, H., Niu, F., 1994. Seismic evidence for a 920-km discontinuity in the mantle. Nature 371, 301–305.
Kellogg, L.H., Hager, B.H., van der Hilst, R.D., 1999. Compositional stratification in the deep mantle. Science 283, 1881–1884.
Kohlstedt, D.L., Keppler, H., Rubie, D.C., 1996. Solubility of water in the α, β and γ phases of $(Mg, Fe)_2SiO_4$. Contrib. Mineralog. Petrol. 123, 345–357.
Korenaga, J., Jordan, T.H., 2004. Physics of multiscale convection in Earth's mantle: evolution of sublithospheric convection. J. Geophys. Res. 109, B01405. doi:10.1029/2003JB002464.
Koyama, T., Shimuzi, H., Utada, H., Ichiki, M., Ichiki, E., Hae, R., 2006. Water content in the mantle transition zone beneath the North Pacific derived from the electrical conductivity anomaly. Earth's Deep Water Cycle.: Geophysics Monograph Series, 168. AGU, pp. 171–180 doi:10.1029/168GM13.
Kubo, T., Ohtani, E., Kondo, T., Kato, T., Toma, M., Hosoya, T., Sano, A., Kikegawa, T., Nagase, T., 2002. Metastable garnet in oceanic crust at the top of the lower mantle. Nature 420, 803–806.
Lawrence, J.F., Shearer, P.M., 2006. A global study of transition zone thickness using receiver functions. J. Geophys. Res. 111. doi:10.1029/2005JB003973.
Lawrence, J.F., Shearer, P.M., 2008. Imaging mantle transition zone thickness with *SdS-SS* finite-frequency sensitivity kernels. Geophys. J. Int. 174, 143–158. doi:10,1111/j.1365-246X.2007.03673.x.
Lawrence, J.F., Wysession, M.E., 2006. Seismic evidence for subduction-transported water in the lower mantle. Earth's Deep-Water Cycle. AGU Monograph, pp. 251–261.
Leahy, G.M., Bercovici, D., 2007. On the dynamics of a hydrous melt layer above the transition zone. J. Geophys. Res. 112, B07401. doi:10.1029/2006JB004631.
Leahy, G.M., Bercovici, D., 2010. Reactive infiltration of hydrous melt above the mantle transition zone. J. Geophys. Res. 115, B08406. doi:10.1029/2009JB006757.
Lebedev, S., Nolet, G., 2003. Upper mantle beneath Southeast Asia from S velocity tomography. J. Geophys. Res. 108. doi:10.1029/2000JB000073.
Lebedev, S., Chevrot, S., van der Hilst, R.D., 2002. The 660-km discontinuity within the subducting NW-Pacific lithospheric slab. Earth Planet. Sci. Lett. 205, 25–35.
Lei, J., Zhao, D., 2005. P-wave tomography and origin of the Changbai intraplate volcano in Northeast Asia. Tectonophysics 397, 281–295.
Li, C., van der Hilst, R.D., 2010. Structure of the upper mantle and transition zone beneath Southeast Asia from traveltime tomography. J. Geophys. Res. 115, B07308.
Li, X., Sobolev, S.V., Kind, R., Yuan, X., Estabrook, C.H., 2000. A detailed receiver function image of the upper mantle discontinuities in the Japan subduction zone. Earth Planet. Sci. Lett. 183, 527–541.
Li, J., Chen, Q.-F., Vanacore, E., Niu, F., 2008. Topography of the 660-km discontinuity and implications for a retrograde motion. Geophys. Res. Lett. 35, L01302. doi:10.1029/2007GL031658.
Litasov, K.D., Ohtani, E., Sano, A., 2006. Influence of water on major phase transitions in the Earth's mantle. Earth's Deep Water Cycle. : Geophysics Monograph Series, 168. AGU, pp. 95–112. doi:10.1029/168GM08.
Mégnin, C., Romanowicz, B., 2000. The 3D shear velocity structure of the mantle from the inversion of body, surface and higher mode waveforms. Geophys. J. Int. 143, 709–728.
Melbourne, T., Helmberger, D., 1998. Fine structure of the 410-km discontinuity. J. Geophys. Res. 103, 10091–10102.
Miyashiro, A., 1986. Hot regions and the origin of marginal basins in the western Pacific. Tectonophysics 122, 122–216 1992.
Nakakuki, T., Tagawa, M., Iwase, Y., 2010. Dynamical mechanisms controlling information and avalanche of a stagnant slab. Phys. Earth Planet. Inter. 183, 309–320.
Neele, F., 1996. Sharp 400-km discontinuity from short-period P reflections. Geophys. Res. Lett. 23, 419–422.
Neele, F., de Regt, H., Van Decar, J., 1997. Gross errors in upper-mantle discontinuity topography from underside reflection data. Geophys. J. Int. 129, 194–204.
Niu, F., Kawakatsu, H., Fukao, Y., 2003. Seismic evidence for a chemical heterogeneity in the midmantle: a strong and slightly dipping seismic reflector beneath the Mariana subduction zone. J. Geophys. Res. 108, B9. doi:10.1029/2002JB002384.
Niu, F., Levander, A., Ham, S., Obayashi, M., 2005. Mapping the subducting Pacific slab beneath southwest Japan with Hi-net receiver functions. Earth Planet. Sci. Lett. 239, 9–17.
Northrup, C.J., Royden, L.H., Burchfiel, B.C., 1995. Motion of the Pacific plate relative to Eurasia and its potential relation to Cenozoic extension along the eastern margin of Eurasia. Geology 23, 719–722.
Obayashi, M., Sugioka, S., Yoshimitsu, J., Fukao, Y., 2006. High temperature anomalies oceanward of subducting slabs at the 410-km discontinuity. Earth Planet. Sci. Lett. 243, 149–158.
Ohtani, E., 2005. Water in the mantle. Elem. 1, 25–30.
Ohtani, E., Sakai, T., 2008. Recent advances in the study of mantle phase transitions. Phys. Earth Planet. Inter. 170, 240–247.
Ohtani, E., Toma, M., Listasov, K., Kubo, T., Suzuki, A., 2001. Stability of dense hydrous magnesium silicate phases and water storage capacity in the transition zone and lower mantle. Phys. Earth Planet. Inter. 124, 115–117.
Okino, K., Ando, M., Kaneshima, S., Hirahara, K., 1989. The horizontally lying slab. Geophys. Res. Lett. 16, 1059–1062.
Press, W.H., Flannery, B.P., Teukolsky, S.A., Vetterling, W.T., 1992. Numerical recipes C: The Art of scientific computing, 2nd Edition. Cambridge University Press, Cambridge, United Kingdom.
Priesley, K., Debayle, McKenzie, D., Pilidou, S., 2006. Upper mantle structure of eastern Asia from multimode surface waveform tomography. J. Geophys. Res. 111, B10304. doi:10.1029/2005JB004082.
Ramesh, D., Kawakatsu, H., Watada, S., Yuan, X., 2005. Receiver function images of the central Chugoku region in the Japanese islands using Hi-net data. Earth Planet. Space 57, 271–280.
Revenaugh, J., Jordan, T.H., 1991. Mantle layering from ScS reverberations: 2. The transition zone. J. Geophys. Res. 96, 19763–19810.
Revenaugh, J., Sipkin, S.A., 1994. Seismic evidence for silicate melt atop the 410-km mantle discontinuity. Nature 369, 474–476.
Ribe, N.M., Sturzmann, E., Ren, Y., van der Hilst, R.D., 2007. Buckling instabilities of subducted lithosphere beneath the transition zone. Earth Planet. Sci. Lett. 254, 173–179.
Richard, G.C., Iwamori, H., 2010. Stagnant slab, wet plumes and Cenozoic volcanism in East Asia. Phys. Earth Planet. Inter. 1–2, 280–287. doi:10.1016/j.pepi.2010.02.009.
Richard, G.C., Bercovici, D., Karato, S., 2006. Slab dehydration in the Earth's mantle transition zone. Earth Planet. Sci. Lett. 251, 156–167.
Romanowicz, B., 2003. Global mantle tomography: progress status in the past 10 years. Annu. Rev. Earth Planet. Sci. 31, 308–328.
Rondenay, S., 2009. Upper mantle imaging with array recordings of converted and scattered teleseismic waves. Surv. Geophys. 30, 377–405.
Roth, E., Wiens, D., Dorman, L., Hildebrand, J., Webb, S., 1999. Seismic attenuation tomography of the Tonga-Fiji region using phase pair methods. J. Geophys. Res. 104, 4795–4810.
Roth, E., Wiens, D., Zhao, D., 2000. An empirical relationship between seismic attenuation and velocity anomalies in the upper mantle. Geophys. Res. Lett. 27, 601–604.
Rychert, C.A., Shearer, P.M., 2009. A global view of the lithosphere–asthenosphere boundary. Science 332, 495–498. doi:10.1126/science.1169754.
Saikia, A., Frost, D.J., Rubie, D.C., 2008. Splitting of the 520-kilometer seismic discontinuity and chemical heterogeneity in the mantle. Science 319, 1515–1518.
Saita, T., Suetsugu, D., Ohtaki, T., Takenaka, H., Kanjo, K., Purwana, I., 2002. Transition zone thickness beneath Indonesia as inferred using the receiver function method for data from JISNET regional broadband seismic network. Geophys. Res. Lett. 29. doi:10.1029/2001GL013629.
Schaeffer, A.J., Bostock, M.G., 2010. A low velocity zone atop the transition zone in northwestern Canada. J. Geophys. Res. 15, B06302. doi:10.1029/2009JB006856.
Schmerr, N., Garnero, E.J., 2006. Investigation of upper mantle discontinuity structure beneath the central Pacific using *SS* precursors. J. Geophys. Res. 111, B08305. doi:10.1029/2005JB004197.
Schmerr, N., Garnero, E.J., 2007. Upper mantle discontinuity topography from thermal and chemical heterogeneity. Science 318, 623–626.
Schmerr, N., Christine Thomas, C., 2011. Subducted lithosphere beneath the Kuriles from migration of PP precursors. Earth Planet. Sci. Lett. 311, 101–111. doi:10.1016/j.epsl.2011.09.002.
Schmid, C., Goes, S., van der Lee, S., Giardini, D., 2002. Fate of the Cenozoic Farallon slab from a comparison of kinematic thermal modeling with tomographic images. Earth Planet. Sci. Lett. 204, 17–32.

Seno, T., Sakurai, T., Stein, S., 1996. Can the Okhotsk plate be discriminated from the North American plate? J. Geophys. Res. 101, 11305–11315.
Shearer, P.M., 1990. Seismic imaging of upper-mantle structure with new evidence for a 520-km discontinuity. Nature 344, 121–126.
Shearer, P.M., 1991. Imaging global body-wave phases by stacking long-period seismograms. J. Geophys. Res. 96, 20353–20364.
Shearer, P.M., 1993. Global mapping of upper mantle reflectors from long-period *SS* precursors. Geophys. J. Int. 115, 878–904.
Shearer, P.M., 1996. Transition zone velocity gradients and the 520-km discontinuity. J. Geophys. Res. 101, 3053–3066.
Shearer, P.M., 2000. Upper mantle seismic discontinuities. Earth's deep interior: mineral physics and tomography from the atomic to the global scale. Geophys. Monogr. 117, 115–131.
Shearer, P.M., Masters, T.G., 1992. Global mapping of topography on the 660 km discontinuity. Nature 355, 791–796.
Shearer, P.M., Flanagan, M.F., Hedlin, A.H., 1999. Experiments in migration processing of *SS* precursor data to image upper mantle discontinuity structure. J. Geophys. Res. 104, 7229–7242.
Shen, X., Zhou, H., Kawakatsu, H., 2008. Mapping the upper mantle discontinuities beneath China with teleseismic receiver functions. Earth Planet. Space 60, 713–719.
Shieh, S.R., Mao, H.-K., Hemley, R.J., Chung Ming, L., 1998. Decomposition of phase D in the lower mantle and the fate of dense hydrous silicates in subducting slabs. Earth Planet. Sci. Lett. 159, 13–23.
Smyth, J.R., Frost, D.J., 2001. The effect of water on the 410-km discontinuity: an experimental study. Geophys. Res. Lett. 29. doi:10.1029/2001GL014418.
Stixrude, L., Lithgow-Bertelloni, C., Kiefer, B., Fumagalli, P., 2007. Phase stability and shear softening in $CaSiO_3$ perovskite at high pressure. Phys. Rev. Lett. B75, 024108.
Suetsugu, D., Inoue, T., Yamada, A., Zhao, D., Obayashi, M., 2006. In: an der Lee, S., Jacobsen, S.D. (Eds.), Towards mapping the three-dimensional distribution of water in the transition zone from P-velocity tomography and 660-km discontinuity depths. : Earth's Deep Water Cycle, 168. American Geophysical Union Monograph Series, pp. 237–249.
Suetsugu, D., Inoue, T., Obayashi, M., Yamada, A., Shiobara, H., Sugioka, H., Ito, A., Kanazawa, T., Kawakatsu, H., Shito, A., Fukao, Y., 2010. Depths of the 410-km and 660-km discontinuities in and around the stagnant slab beneath the Philippine Sea: is water stored in the stagnant slab? Phys. Earth Planet. Inter. 183, 270–279.
Sugioka, H., Suetsugu, D., Obayashi, M., Fukao, Y., Gao, Y., 2010. Fast P and S wave velocities associated with the "cold" stagnant slab beneath the northern Philippine Sea. Phys. Earth Planet. Inter. 179, 1–6. doi:10.1016/j.pepi.2010.01.006.
Sung, C.-M., Burns, R.G., 1976. Kinetics of high-pressure phase transformations: implications to the evolution of the olivine–spinel transition in the downgoing lithosphere and its consequences on the dynamics of the mantle. Tectonophysics 31, 1–32.
Tagawa, M., Nakakuki, T., Tajima, F., 2007. Dynamical modeling of trench retreat driven by the slab interaction with the mantle transition zone. Earth Planets Space 59, 65–74.
Tateno, S., Hirose, K., Sata, N., Ohishi, Y., 2005. Phase relations in $Mg_3Al_2Si_3O_{12}$ to 180 GPa: effect of Al on post-perovskite phase transition. Geophys. Res. Lett. 32, L15306. doi:10.1029/2005GL023309.
Tauzin, B., Debayle, E., Wittlinger, G., 2008. The mantle transition zone as seen by global *Pds* phases: no clear evidence for a thin transition zone beneath hotspots. J. Geophys. Res. 113, B08309. doi:10.1029/2007JB005364.
Tauzin, B., Debayle, E., Wittlinger, G., 2010. Seismic evidence for a global low velocity layer in the Earth's upper mantle. Nat. Geosci. 3, 718–721. doi:10.1038/NGEO969.
Tetzlaff, M., Schmeling, H., 2000. The influence of olivine metastability on deep subduction of oceanic lithosphere. Phys. Earth Planet. Inter. 120, 29–38.
Tibi, R., Wiens, D.A., Shiobara, H., Sugioka, H., Yuan, X., 2007. Double seismic discontinuities at the base of the mantle transition zone. Geophys. Res. Lett. 34, L16316. doi:10.1029/2007GL030527.
Tonegawa, T., Hirahara, K., Shibutani, T., Fujii, N., 2006. Lower slab boundary in the Japan subduction zone. Earth Planet. Sci. Lett. 247, 101–107.
Torii, Y., Yoshioka, S., 2007. Physical conditions producing slab stagnation: constraints of the Clapeyron slope, mantle viscosity, trench retreat, and dip angles. Tectonophysics 445, 200–209.
Vacher, P., Mocquet, A., Sotin, C., 1998. Computation of seismic profiles from mineral physics: the importance of the non-olivine components for explaining the 660 km depth discontinuity. Phys. Earth Planet. Inter. 106, 275–298.
van der Hilst, R., Engdahl, R., Spakman, W., Nolet, G., 1991. Tomographic imaging of subducted lithosphere below northwest Pacific island arcs. Nature 353, 37–43.
van der Hilst, R.D., Widiyantoro, S., Engdahl, E.R., 1997. Evidence for deep mantle circulation from global tomography. Nature 386, 578–584.
van der Meijde, M., Marone, F., Giardini, D., van der Lee, S., 2003. Seismic evidence for water deep in Earth's upper mantle. Science 300, 1556–1558.
van der Meijde, M., van der Lee, S., Giardini, D., 2005. Seismic discontinuities in the Mediterranean mantle. Phys. Earth Planet. Inter. 148, 233–250.
van Keken, P.E., Karato, S., Yuen, D.A., 1996. Rheological control of oceanic crust separation in the transition zone. Geophys. Res. Lett. 23, 1821–1824.
Vidale, J.E., Benz, H.M., 1992. Upper-mantle seismic discontinuities and the thermal structure of subduction zones. Nature 356, 678–683.
Vidale, J.E., Ding, X.-Y., Grand, S.P., 1995. The 410-km-depth discontinuity: a sharp estimate from near-critical reflections. Geophys. Res. Lett. 22, 2557–2560.
Wang, Y., Uchida, T., Zhang, J., Rivers, M.L., Sutton, S.R., 2004. Thermal equation of state of akimotite MgSiO3 and effect of akimotite–garnet transformation on seismic structure near the 660 km discontinuity. Phys. Earth Planet. Inter. 143–144, 57–80.
Weidner, D., Wang, Y., 1998. Chemical- and Clapeyron-induced buoyancy at the 660 km discontinuity. J. Geophys. Res. 103, 7431–7441.
Weidner, D., Wang, Y., 2000. Phase transformations; implications for mantle structure. In: Karato, S., Forte, A., Liebermann, R., Masters, G., Stixrude, L. (Eds.), Earth's Deep Interior: Mineral Physics and Tomography from the Atomic to Global Scale. American Geophysical Union, pp. 215–235.
Widiyantoro, S., Kennett, B.L.N., van der Hilst, R.D., 1999. Seismic tomography with P and S data reveals lateral variations in the rigidity of deep slabs. Earth Planet. Sci. Lett. 173, 91–100.
Wood, B.J., 1995. The effect of H_2O on the 410-kilometer seismic discontinuity. Science 268, 74–76.
Xu, Y., Wiens, D.A., 1997. Upper mantle structure of the southwest Pacific from regional waveform inversion. J. Geophys. Res. 102, 27439–27451.
Yamada, A., Zhao, D., Inoue, T., Suetsugu, D., Obayashi, M., 2009. Seismological evidence for compositional variations at the base of the mantle transition zone under Japan islands. Gondwana Res. doi:10.1016/j.gr.2009.04.009.
Zhao, D., 2001. Seismological structure of the subduction zones and its implication for arc magmatism and dynamics. Phys. Earth Planet. Inter. 127, 197–214.
Zhao, D., 2004. Global tomographic images of mantle plumes and subducting slabs: insight into deep Earth dynamics. Phys. Earth Planet. Inter. 146, 3–34.
Zhao, D., Ohtani, E., 2009. Deep slab subduction and dehydration and their geodynamic consequences: evidence from seismology and mineral physics. Gondwana Res. 16, 401–413.
Zhao, D., Hasegawa, A., Horiuchi, S., 1992. Tomographic imaging of P and S wave velocity structure beneath northeastern Japan. J. Geophys. Res. 97, 19909–19928.
Zhao, D., Maruyama, S., Omori, S., 2007. Mantle dynamics of Western Pacific and East Asia: insight from seismic tomography and mineral physics. Gondwana Res. 1, 120–131.
Zheng, Y., Lay, T., Flanagan, M.P., Williams, Q., 2007. Pervasive seismic wave reflectivity and metasomatism of the Tonga mangle wedge. Science 316. doi:10.1126/science.1138074, 2007.
Zhu, G., Shi, Y., Tackley, P., 2010. Subduction of the Western Pacific Plate underneath Northeast China: implications of numerical studies. Phys. Earth Planet. Inter. 178, 92–99.
Zou, H.B., Fan, Q.C., Yao, Y.P., 2008. U-Th systematics of dispersed young volcanoes in NE China: asthenosphere upwelling caused by pilling and upward thickening of stagnant Pacific slab. Chem. Geol. 255, 134–142.